Image charge effects in single-molecule junctions: Breaking of symmetries and negative-differential resistance in a benzene single-electron transistor

K. Kaasbjerg[1,*] and K. Flensberg[2]

[1]*Center for Atomic-scale Materials Design (CAMD), Department of Physics, Technical University of Denmark,*
DK-2800 Kgs. Lyngby, Denmark
[2]*Niels Bohr Institute and Nano-Science Center, University of Copenhagen, Universitetsparken 5, DK-2100 Copenhagen, Denmark*

Both experiments and theoretical studies have demonstrated that the interaction between the current-carrying electrons and the induced polarization charge in single-molecule junctions leads to a strong renormalization of molecular charging energies. However, the effect on electronic excitations and molecular symmetries remain unclear. Using a theoretical framework developed for semiconductor-nanostructure-based single-electron transistors (SETs), we demonstrate that the image charge interaction breaks the molecular symmetries in a benzene-based single-molecule transistor operating in the Coulomb blockade regime. This results in the appearance of a so-called blocking state, which gives rise to negative-differential resistance (NDR). We show that the appearance of NDR and its magnitude in the symmetry-broken benzene SET depends in a complicated way on the interplay between the many-body matrix elements, the lead tunnel coupling asymmetry, and the bias polarity. In particular, the current reducing property of the blocking state causing the NDR is shown to vanish under strongly asymmetric tunnel couplings, when the molecule is coupled stronger to the drain electrode. The calculated *I*-*V* characteristic may serve as an indicator for image charge broken molecular symmetries in experimental situations.

PACS number(s): 73.23.Hk, 73.63.Rt

I. INTRODUCTION

Over the past decade the field of single-molecule electronics has experienced significant progress both experimentally and theoretically. On the experimental side break-junction and electromigration techniques have become standard ways of realizing nanoscale junctions with only one molecule bridging the gap between the source and drain electrodes.[1–3] With the coupling between the molecule and the electrodes often being a highly uncontrollable parameter, the transport through single-molecule junctions spans different parameter regimes depending on the fabrication techniques.[4] Three-terminal measurements where the molecule couples capacitively to a third gate electrode most often end up in the weak-coupling regime where the Coulomb blockaded transport through the molecule is dominated by sequential tunneling. In these setups, the coupling to the gate electrode allows control of the alignment between the molecular levels and the Fermi levels of the leads. The *I*-*V* characteristics are therefore often summarized in the so-called charge stability diagram, which maps out the differential conductance dI/dV_{sd} as a function of the gate and source-drain voltage. These diagrams help to understand the excitations intrinsic to the molecule, as for example the vibrational degrees of freedom.[2,5]

One still unresolved issue is how the junction polarization resulting from the charging of the molecule influences the molecular states. In, for example, three-terminal electro-migrated nanoscale junctions,[2,3] where the dimensions of the source and drain electrodes are large compared to the metallic screening length, this effect can be expected to be significant. So far, both experiments[6,7] and theoretical simulations[8,9] have demonstrated that the interaction with the polarization charge—the so-called image charges—leads to a strong renormalization of the molecular charging energies. In

a charge-stability diagram, this is reflected in addition energies reduced with up to several electron volts compared to the value expected from gas phase level positions of the molecule. On the other hand, the effect on excited states remain unresolved. A number of experimental studies have indicated image charge stabilized states close to the electrodes and modified excitation energies.[7,10] Hence, a thorough investigation of the image charge effect and its influence on model parameters can help to improve the interpretation of experimental observations.

With the recent interest in the role of molecular degeneracies in the Coulomb blockade regime,[11–13] it is of relevance to address the effect on such degeneracies. While splittings of degenerate levels on the order of the tunnel broadening results in quasidegenerate states that still behave as being degenerate, a larger splitting completely destroys interference effects and the associated signature in the transport characteristics.[11,13] Degeneracies also play an important role in Jahn-Teller active molecules that undergo distortions upon charging. Here, the higher dimensional adiabatic potential energy surface of the charged molecule resulting from the coupling to the Jahn-Teller active vibrations leads to distinct transport characteristics.[14,15] Also in this case can a splitting of the degenerate levels result in a qualitatively different signature in the stability diagram. For example, a transport signature characteristic of the pseudo–Jahn-Teller effect might result when the size of the energy splitting matches a multiple of a vibrational energy.[16]

In this paper, we present a quantitative study of the impact on molecular degeneracies by studying the image charge effect in a benzene-based single-molecule junction. Despite the presence of the Jahn-Teller effect in the benzene molecule,[17] we will focus on the splitting of the electronic states due to image charge effects and neglect any coupling to vibrations.

Recent theoretical studies have already touched upon the image charge effect and other symmetry-breaking agents in a benzene SET, however, without taking into account the full interaction between the molecule and the image charges.[11,18] Here, the purpose is twofold. First, we present a general framework that has previously been used to account for image charge effects in semiconductor nanostructures[19] and discuss its applicability for single-molecule junctions operating in the Coulomb blockade regime. Second, the implication on the degeneracies of the benzene molecule and the consequence for the low-bias transport characteristics are investigated. We find that the image charge effect indeed breaks the high symmetry of the molecule and leads to a large splitting (∼40−80 meV) of the degenerate ground state of the singly charged molecule.

Due to a breakdown of the transport selection rules that apply in the isolated molecule, the symmetry-split excited state of the charged molecule is turned into a so-called blocking state. As a consequence, an NDR feature appears at a bias corresponding to the level splitting. The stability of the NDR feature with respect to an asymmetry in the lead couplings and the coupling site on the molecule is analyzed. Similar NDR features caused by radiative relaxation to a blocking state[20] and an interference-induced blocking state[11,21] have been reported previously in the literature for the benzene SET. Contrary to these cases, the NDR feature observed here is exclusively caused by the broken symmetry of the molecule and needs none of these additional effects to occur.

The paper is organized as follows. Section II presents the theoretical approach used to describe the image charge effect in this work. This involves a generalized Hamiltonian for the molecule with extra terms originating from the interaction with the image charges. In Sec. III, the benzene SET and the semiempirical Pariser-Parr-Pople Hamiltonian are introduced. Furthermore, an analysis of the broken symmetry and the accompanying splitting of the degenerate molecular states together with a condition for the occurrence of NDR is given. The resulting low-bias *I-V* characteristics are presented and analyzed in Sec. IV. Finally, Sec. V summarizes our findings and points to other situations where the image charge effect may be important in single-molecule junctions.

II. JUNCTION HAMILTONIAN AND THE CURRENT

In the following section, we present a general framework for the description of single-molecule junctions operating in the Coulomb blockade regime, i.e., with a weak tunnel coupling between the molecule and the leads. While different approaches to the calculation of the current to different orders in the leads couplings have been given elsewhere,[22] the present study focuses on the interaction with the image charges in the junction environment. Figure 1(a) illustrates an idealized setup for such a three-terminal junction with the molecule lying on a gate oxide between the source and drain electrodes. With the molecule playing the role of the quantum dot, this type of single-molecule junction is very similar to multiterminal-semiconductor-based quantum dot structures, where the theoretical description of image charges and their influence on the dot states is well established.[19]
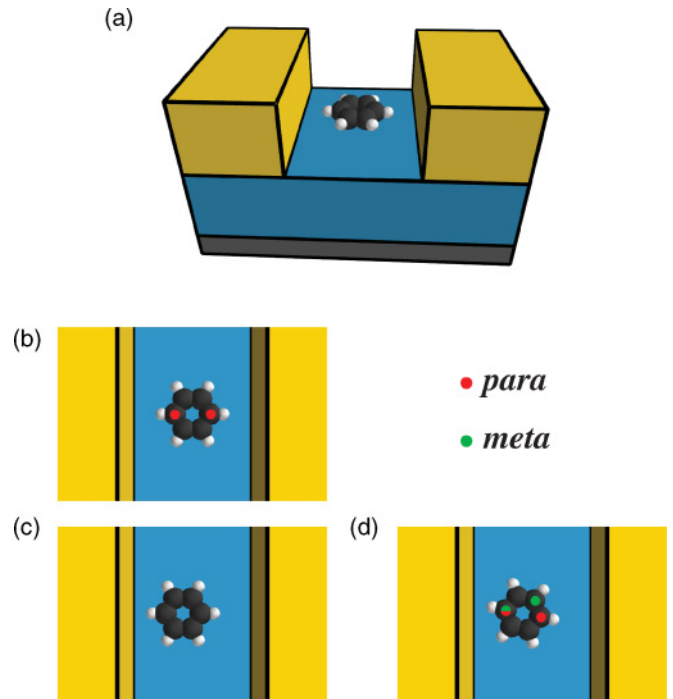

FIG. 1. (Color online) Schematic illustration of a benzene single-electron transistor. (a) Side view of the nanojunction with the molecule positioned on the gate dielectric between the source and drain electrodes. The capacitive coupling between the gate electrode (gray) at the bottom and the molecule provides control over the energy levels of the molecule. (b)–(d) Top view of the junction with the molecule positioned in different configurations. The red and green dots indicate the coupling sites for coupling in the para and meta configurations, respectively. (b) Symmetric setup with the molecule positioned in the middle of the gap between the electrodes. (c) Asymmetric setup with the molecule positioned closer to the left electrode. (d) Same as in (c) but with an additional rotation of the molecule. Due to the interaction with the image charges of the junction, the rotation of the molecule breaks all the symmetries of the molecular Hamiltonian and results in qualitatively different *I-V* characteristics and NDR.

The theoretical framework is based on a macroscopic description of the metallic electrodes and the surrounding dielectric, while the quantum dot(s) is described quantum mechanically.

It is here illustrated how the same formalism can be applied to a single-molecule junction. We briefly summarize the most important aspects of the approach and explain in detail the appearance of new terms in the molecular Hamiltonian that result from the image charge effect. The validity of a macroscopic electrostatic description for single-molecule SETs is also discussed.

A. Hamiltonian

A general Hamiltonian for a single-molecule junction including the image charge effect can be written as the sum of

the following terms:

$$H = H_{\text{mol}} + H_{\text{T}} + H_{\text{leads}} + H_{\text{mol}-\text{env}} + H_{\text{env}}. \quad (1)$$

Here, H_{mol} denotes the Hamiltonian of the molecule expressed in a basis of atomic orbitals ϕ_i with corresponding creation and annihilation operators $\{c_{i\sigma}^{\dagger}, c_{i\sigma}\}$. In the present work, this basis will be the atomic p_z orbitals of the carbon atoms in the benzene molecule. The next two terms account for the tunnel couplings to the lead (labeled by α) electrons,

$$H_{\text{T}} + H_{\text{leads}} = \sum_{k\sigma\alpha} t_{k\sigma}^{\alpha} c_{k\sigma\alpha}^{\dagger} c_{\alpha\sigma} + \text{H.c.} + \sum_{k\sigma\alpha} \varepsilon_{k\sigma}^{\alpha} c_{k\sigma\alpha}^{\dagger} c_{k\sigma\alpha}.$$

$$(2)$$

For simplicity, it is here assumed that only one orbital ϕ_{α} on the molecule couples to each of the left ($\alpha = L$) and right ($\alpha = R$) leads.

The remaining two terms in Eq. (1) account for the electrostatic energy arising from the interaction between the charge of the molecule and junction. This includes the interaction with the induced polarization charge in the environment due to charging of the molecule (the image charges), the energy of the molecule in the potential from voltages V_i applied to the electrodes, and the electrostatic energy of the capacitively coupled electrodes of the junction. For now, these two terms are most conveniently expressed together with the molecular Hamiltonian H_{mol} in real space and first quantization as[19]

$$H_{\text{mol}} + H_{\text{mol}-\text{env}} + H_{\text{env}} = \frac{1}{2m}\sum_{n=1}^{N} \nabla_n^2 - e\sum_{n=1}^{N} V(\mathbf{r}_n) + \frac{e^2}{2}\sum_{n=1}^{N}\sum_{n'\neq n}^{N} G(\mathbf{r}_n, \mathbf{r}_{n'}) + \sum_{ij} V_i C_{ij} V_j, \quad (3)$$

where m is the electron mass, N is the number of electrons on the molecule, G denotes the electrostatic Green's function of the junction, and C_{ij} is the capacitance matrix of the junction coupling the charge on the different electrodes. The single-particle potential V is given by

$$V(\mathbf{r}) = -\frac{e}{2}\widetilde{G}(\mathbf{r},\mathbf{r}) + \int d\mathbf{r}' G(\mathbf{r},\mathbf{r}')\rho_{\text{ion}}(\mathbf{r}') + \sum_{i} \alpha_i(\mathbf{r})V_i,$$

$$(4)$$

where $\widetilde{G}$ is the part of the Green's function that accounts for the induced potential due to an electron in $\mathbf{r}$ (see below), ρ_{ion} is the charge distribution of ionic cores of the molecule (often described by a pseudopotential in *ab initio* approaches), and α_i is an electrode specific function, which gives the spatial profile of the junction potential with a unit voltage applied to the ith electrode and in the absence of the molecule. The α functions are solutions to the Laplace equation

$$-\nabla \cdot [\epsilon_0 \varepsilon_{\text{r}}(\mathbf{r})\nabla\alpha_i(\mathbf{r})] = 0 \quad (5)$$

with boundary conditions $V_j = \delta_{ij}$ at the electrodes; ε_{r} is the spatially varying dielectric constant of the junction, and ϵ_0 is the vacuum permittivity.

Apart from the capacitive energy in last term of Eq. (3) and the contribution from the applied voltages in the last term of Eq. (4), the Hamiltonian in Eq. (3) bears close resemblance to the usual many-body Hamiltonian for interacting electrons moving in an external potential. However, the electrostatic Green's function plays an important role in this modified Hamiltonian. It is seen to have replaced the Coulomb interaction [third and second terms of Eqs. (3) and (4), respectively] and results in an additional single-particle term [first term of Eq. (4)].

The electrostatic Green's function solves Poisson's equation with a δ-function source term,

$$-\nabla \cdot [\epsilon_0 \varepsilon_{\text{r}}(\mathbf{r})\nabla G(\mathbf{r},\mathbf{r}')] = \delta(\mathbf{r} - \mathbf{r}') \quad (6)$$

with Dirichlet boundary conditions $V_i = 0$. For a given junction geometry the Green's function gives the potential in $\mathbf{r}$ due to a unit charge in $\mathbf{r}'$. When both $\mathbf{r}$ and $\mathbf{r}'$ belong to the vacuum region of the junction where the molecule resides, the Green's function can be written as a sum of the direct (unscreened) Coulomb interaction plus a contribution $\widetilde{G}$ from the image charges (screening),

$$G(\mathbf{r},\mathbf{r}') = \frac{1}{|\mathbf{r} - \mathbf{r}'|} + \widetilde{G}(\mathbf{r},\mathbf{r}'). \quad (7)$$

The replacement of the Coulomb interaction with the electrostatic Green's function in Eqs. (3) and (4) therefore corresponds to a screening of the Coulomb interaction by the polarization response of the junction (the image charges). The additional single-particle term in Eq. (4) has the form of an electronic self-interaction given by the $\widetilde{G}$ part of the Green's function. This is the energy of the electron in its own induced potential, i.e., the interaction between the electron and its own image charge. For the standard example of a point charge positioned at a distance z from an infinite conducting surface this term reduces to the classical $-1/4z$ energy well known from classical electrostatics.[23]

In the present work, the electrostatic Green's function is obtained for the simplified junction geometry discussed in Appendix A. This allows for an analytical solution of Poisson's equation in Eq. (6). It has been verified that this gives a very good description of the potential in the realistic junction in Fig. 1.[9] The spatial profiles of the source-drain and gate voltages follow from the α functions which are solutions to Laplace equation in Eq. (5). For simplicity, we approximate these by simple linear functions. The coupling to the gate electrode is set to unity, i.e., $\alpha_{\text{gate}} = 1$. In realistic descriptions of the gate potential and in experimental realizations of nanoscale junctions this number is often rather low ($\sim 0.1-0.2$)[6,7,9,24] and may vary over the spatial extend of the molecule.[9] However, under the assumption that the

gate potential is constant on the molecule, the gate-coupling parameter only serves as a scaling factor for the shift of the molecular energy levels. The source-drain voltage is modeled by a linear ramp between the two electrodes with the voltage applied symmetrically to the left and right electrode,

$$V(z) = \frac{V_{sd}}{2} - V_{sd}\frac{z}{L}, \tag{8}$$

where $z = 0$ corresponds to the position of the left electrode and L is the electrode spacing. With the chemical potentials of the leads given by

$$\mu_L = E_f - eV_{sd}/2 \quad \text{and} \quad \mu_R = E_f + eV_{sd}/2, \tag{9}$$

where E_f is the equilibrium Fermi level, the positive current direction is from left to right. Within a microscopic description of both the leads and the molecule, the alignment between the lead Fermi levels and the molecular levels follows directly. However, for the simplified description of the leads adopted here, the alignment is treated as a parameter, and the equilibrium Fermi levels are chosen to reside in the middle of the gap of the benzene molecule. The level alignment is illustrated schematically in Fig. 3(b) for a situation with voltages applied to the electrodes.

B. Validity of an electrostatic description

The classical electrostatic treatment of the junction environment in the Hamiltonian in Eq. (1) relies on certain assumptions. First of all, the dimensions of the electrodes and gate dielectric need to be larger than the screening lengths in the respective materials in order for a classical description to be valid. Second, the classical treatment of the environment assumes that there is no significant overlap between the quantum mechanical region and the environment. In the Coulomb blockade regime, this seems to be a fair assumption. Last, since the environment is described with electrostatics, the time scale of the electrons on the molecule needs to be slower than the response times of the metallic electrodes and gate dielectric. This requires the hopping integrals t on the molecule to be smaller than typical values for the plasmon and phonon energies. With molecular level spacing being on the order of eV for conjugated molecules, this is not necessarily the case. Nevertheless, the current-carrying electrons have residence times on the molecule much longer than the response time of the environment. So the question is not whether or not the image charge effect should be included, but rather if it should be treated as an instantaneous interaction as in Eq. (3) or at the level of mean-field theory where the environment only sees the mean occupation of the electrons on the molecule. In the following we pursue the first direction. We have verified that a mean-field treatment at the level of Hartree-Fock does not change the main conclusions of the present work.

C. Current

We shall here focus on the weak-coupling regime where the occupation probabilities of the molecular states and the current can be obtained within a master equation approach. In the case of degeneracies between the molecular states, a master equation for the density matrix that retains the coherence between the degenerate states must be considered.[13,21] However,

it turns out that in the present study such degeneracies are broken by the interaction with the image charges in the junction environment, which leaves the simpler rate-equation approach valid, so that only the diagonal elements of the reduced density matrix need to be retained.[25,26]

To lowest order in the coupling between the molecule and the leads in Eq. (2), the transition rate between the ith N-electron state and the jth $(N + 1)$-electron state due to tunneling from lead α is given by Fermi's golden rule

$$\Gamma^{\alpha\sigma}_{\substack{N+1,j \\ N,i}} = \frac{2\pi}{\hbar}\gamma^{\alpha\sigma}_{j,i}(N)f_\alpha(E_{ij}), \tag{10}$$

where f_α is the Fermi distribution for the lead electrons, $E_{ij} = E_j^{N+1} - E_i^N$ corresponds to the molecular ionization energies and electron affinities, and

$$\gamma^{\alpha\sigma}_{j,i}(N) = \rho_\alpha t_\alpha^2 |\langle N + 1, j|c_{\alpha\sigma}^\dagger|N,i\rangle|^2 \tag{11}$$

is the product of the lead density of states ρ_α, the tunnel coupling t_α, and the transition matrix element between the two molecular states involved in the addition of an electron to the molecule from lead α. For the opposite process where an electron tunnels from the molecule to the drain electrode, the transition rate is given by

$$\Gamma^{\alpha\sigma}_{\substack{N-1,j \\ N,i}} = \frac{2\pi}{\hbar}\gamma^{\alpha\sigma}_{i,j}(N-1)[1 - f_\alpha(E_{ij})], \tag{12}$$

where the Fermi factor ensures that there is an empty state in the lead. We here restrict our discussion to the case of identical left and right leads, modeled by normal metals with a constant density of states. The presence of a fast (on the scale of the time between tunneling events) energy relaxation mechanism in the leads justifies the equilibrium description of the lead electrons in Eqs. (10) and (12).

The rate equations for the occupations of the molecular states now read

$$\dot{P}_{N,i} = \sum_{\alpha,j} \Big[-P_{N,i}\big(\Gamma^\alpha_{\substack{N+1,j \\ N,i}} + \Gamma^\alpha_{\substack{N-1,j \\ N,i}}\big)$$
$$+ P_{N+1,j}\Gamma^\alpha_{\substack{N,i \\ N+1,j}} + P_{N-1,j}\Gamma^\alpha_{\substack{N,i \\ N-1,j}} \Big]. \tag{13}$$

Together with the normalization condition $\sum_{N,i} P_{N,i} = 1$ the rate equations can be solved in steady state, i.e., $\dot{P}_{N,i} = 0$, for the occupation probabilities $P_{N,i}$. From the steady-state occupations, the current through the molecule follows by evaluating the total rate of electrons from lead α

$$I_\alpha = \mp e \sum_{N,ij} \big(P_{N,i}\Gamma^\alpha_{\substack{N+1,j \\ N,i}} - P_{N,i}\Gamma^\alpha_{\substack{N-1,j \\ N,i}}\big) \tag{14}$$

for $\alpha = L/R$, respectively.

The main objective is here to demonstrate how the inclusion of the image charge effect affects the molecular states and thereby also the I-V characteristic of the molecular junction. For this purpose, the energies and states appearing in Eqs. (10), (11), and (12) must be calculated on the basis of the junction Hamiltonian in Eq. (3) which fully accounts for the interaction with the image charges. The extent to which specific molecular properties are affected is highly dependent on the molecule of interest and its configuration in the nanojunction. A general discussion is therefore not possible;

the rest of the paper seeks to address the importance of the image charge effect in the often studied benzene SET.[11,20,21]

III. BENZENE SET

In the remainder of the paper we consider the transport through the benzene SET illustrated in Fig. 1(a). It has the molecule lying flat on a gate oxide between the source and drain electrodes. The dielectric constant of the gate oxide is set to $\varepsilon_r = 10$ corresponding to the high-κ dielectric Al_2O_3.

In experimental situations both the position of the molecule and the electrode spacing are highly uncontrollable parameters. We therefore consider different setups where the position and orientation of the molecule with respect to the electrodes are varied. In the symmetric setup shown in Fig. 1(b), the molecule is placed in the middle of the junction with the two end atoms facing the electrodes.[27] In this reference setup, the distance between the hydrogen atoms facing the electrodes at the ends of the molecule and the electrostatic boundaries of the electrodes is set to 1.2 Å. With the so-called image charge plane lying ∼1.0 Å outside the outermost atomic layer of a surface,[28] this corresponds to a weak bond between the surface atoms of the electrodes and the benzene molecule (see also Appendix A). To account for the longer range of the p_z orbitals on the carbon atoms, the distance to the gate dielectric is chosen slightly larger to 2 Å. In the following, all changes will be with respect to the above described reference setup.

In order to model experimentally more relevant situations, we also consider the following two setups and combinations hereof. In the first, the molecule is rotated by an angle θ with respect to its symmetric setup in Fig. 1(b) around its sixfold rotational symmetry axis perpendicular to the plane of the molecule. In the second, an asymmetric setup where the distance to one of the electrodes is increased to twice the distance in the reference setup is considered. This leads to a smaller image charge interaction with the most distant electrode. While the symmetric setup corresponds to electrode couplings in the para configuration (marked by red dots in Fig. 1), coupling also in the meta configuration (green dots in Fig. 1) is likely to occur in the asymmetric setup where the relative difference in the distance between the distant electrode and the two coupling sites is smaller. The combination of the above described situations is shown in Fig. 1(d), where the molecule is placed in a rotated position closer to the left electrode.

A. Pariser-Parr-Pople Hamiltonian

In conjugated molecules the sp^2 hybridization of the carbon atom results in an energy separation between the bonding σ orbitals and the higher lying π orbitals which have mainly p_z character. Quantitative predictions of the low energy excitations can therefore be obtained with the simple Pariser-Parr-Pople[29–31] (PPP) description. The PPP Hamiltonian which includes only the π-electron system is given by

$$H_{mol} = \sum_{i\sigma} \varepsilon_{i\sigma} \hat{n}_{i\sigma} - \sum_{\langle ij \rangle \sigma} t_{ij} [c_{i\sigma}^\dagger c_{j\sigma} + \text{H.c.}]$$
$$+ \frac{1}{2} \sum_{i \neq j} V_{ij} (\hat{n}_i - Z_i)(\hat{n}_j - Z_j) + \sum_i U_i \hat{n}_{i\uparrow} \hat{n}_{i\downarrow},$$
$$(15)$$

where $\hat{n}_i = \hat{n}_{i\uparrow} + \hat{n}_{i\downarrow}$ and $Z_i = 1$ are the occupation and valence, respectively, of the p_z orbital at the carbon site i of the molecule. Apart from hopping between the p_z orbitals on neighboring sites in the second term, the PPP description also includes on-site and long-ranged Coulomb interactions between the π electrons. Due to the effective π electron description, the parameters U and V cannot be identified with the usual matrix elements of the Coulomb interaction since screening effects from the σ electrons reduce the Coulomb interaction. Here, the Ohno parametrization[32] is used for the long-ranged Coulomb interactions,

$$V_{ij} = \frac{U}{\sqrt{1 + (\alpha r_{ij})^2}}, \quad (16)$$

where $\alpha = U/(14.397 \,\text{eV Å})$ and r_{ij} is the distance between the carbon sites i and j. It ensures that the bare Coulomb interaction is recovered for large distances, i.e., $V_{ij} \to 1/r$ as $r_{ij} \to \infty$, while for shorter distances the (screened) on-site Coulomb interaction U is approached. The remaining parameters of the PPP Hamiltonian in Eq. (15) have been chosen as $\varepsilon_i = 0$ eV, $t = 2.539$ eV, and $U = 10.06$ eV. This set of parameters has been fitted to experimental excitation energies and hence gives a quantitative description of the excitations in the benzene molecule.[33] We note that in previous studies of Coulomb blockade transport through the benzene molecule,[11,20,21] different sets of parameters have been used. The excitation spectrum of the isolated benzene molecule reported here might therefore differ slightly from these other works. It should be stressed that despite the large value of the on-site Coulomb interaction U, the inclusion of long-ranged Coulomb interactions V_{ij} in the PPP description results in weakly correlated states that to a good approximation can be described with Hartree-Fock theory.[34]

The PPP Hamiltonian in Eq. (15) describes only the isolated molecule. In order to include the interaction with the junction environment, the terms in the Hamiltonian in Eq. (3) involving the $\widetilde{G}$ part of the Green's function and the applied voltages V_i must be taken care of separately. The conversion of these terms from the real-space representation in Eq. (3) to the atomic p_z orbital basis of the PPP Hamiltonian in Eq. (15) is given in Appendix B. This leads to the following additional terms:

$$H_{mol-env} + H_{env} = \sum_{i\sigma} \left[\widetilde{V}_i^{\text{ion}} + \frac{1}{2} \widetilde{V}_{ii} + V_i^{\text{ext}} \right] \hat{n}_{i\sigma}$$
$$+ \frac{1}{2} \sum_{i \neq j} \widetilde{V}_{ij} \hat{n}_i \hat{n}_j + \sum_i \widetilde{V}_{ii} \hat{n}_{i\uparrow} \hat{n}_{i\downarrow}, \quad (17)$$

where $\widetilde{V}_i^{\text{ion}}$, V_i^{ext}, and $\widetilde{V}_{ij}$ are the matrix elements of the induced junction potential $\widetilde{V}_{\text{ion}}$ due to the ionic cores, the matrix element of the external potential $V_{\text{ext}} = \sum_i \alpha_i V_i$ from the applied voltages V_i, and the two-particle matrix elements of $\widetilde{G}$ in the basis of the atomic p_z orbitals, respectively. In order to adapt to the level of complexity of the PPP Hamiltonian, only the diagonal matrix elements of the terms in Eq. (17) are retained here. This should not affect the main conclusions of the paper.

As is evident from Eq. (17), the interaction with the image charges leads to a renormalization of both the onsite energies and the Coulomb interaction. The two first terms inside the
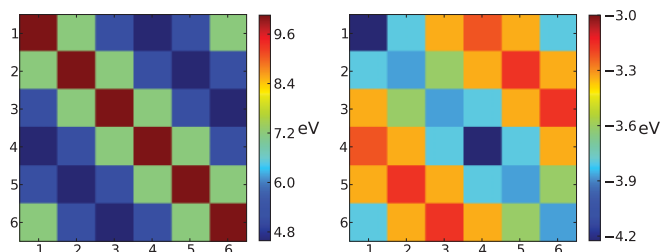
FIG. 2. (Color online) Matrix elements (in eV) of the Coulomb interaction, given by the Ohno parametrization in Eq. (16) (left), and the image charge interaction $\widetilde{V}_{ij}$ in Eq. (17) (right). The numbers on the axes denote the site indices of the carbon atoms in the benzene molecule with sites 1 and 4 corresponding to the carbon sites marked with red dots in Fig. 1(b). The large value of the matrix elements of the image charge interaction results in a significant renormalization of the benzene Hamiltonian and a breaking of its high sixfold rotational symmetry.
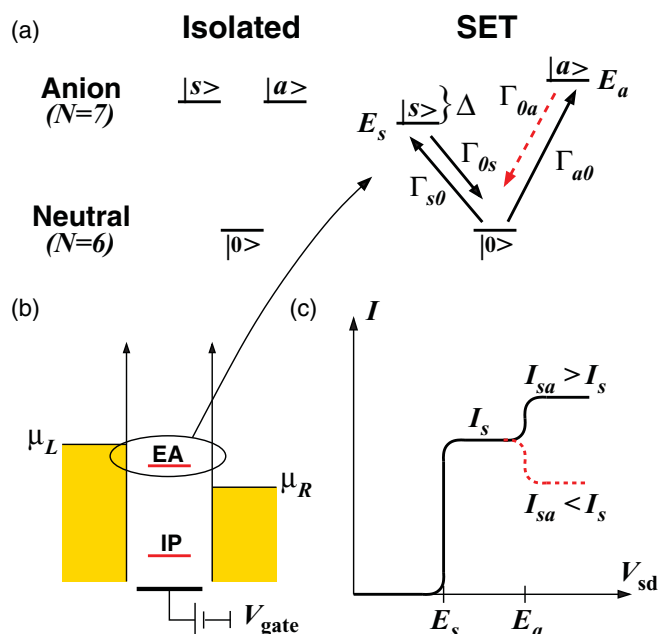

FIG. 3. (Color online) Schematic overview of the states and transport characteristics of the benzene SET. (a) States of the benzene molecule important for the low-bias transport through the molecule. In the SET environment (right), the image charge effect lifts the degeneracy of the anionic ground state of the isolated molecule (left) producing a splitting Δ between the two states labeled $|s\rangle$ and $|a\rangle$ (see text). The transition rates Γ between the states are indicated with arrows. The transition marked with the (red) dashed arrow is responsible for the occurrence of NDR. (b) Alignment between the molecular levels and the the Fermi levels of the leads in an out-of-equilibrium situation. (c) Current as a function of source-drain voltage. With state $|a\rangle$ being a so-called blocking state with a slow exit rate illustrated by the dashed red arrow in (a), it is likely to produce an NDR feature when introduced in the bias window.

square brackets stem from the image charge of the ions and the image charge of the electron itself. The third term inside the brackets is the shift in the on-site energies due to the applied voltages. The two last terms in the last line account for the interaction with the image charges from all the other electrons. These terms have the usual form of the Coulomb interaction and thus correspond to a renormalization of the interactions of the bare molecule in Eq. (16).

The matrix elements of the Coulomb interaction in Eq. (16) and the image charge interaction $\widetilde{V}_{ij}$ (see Appendix B for details) are shown in Fig. 2 for the symmetric setup. As can be seen, the matrix elements of the image charge interaction is on the order of several electron volts and therefore result in a strong renormalization of the Coulomb interactions on the molecule. With the large renormalization of both the on-site energies and the Coulomb interaction in the molecular Hamiltonian in Eq. (15), its is not surprising that the image charge effect has a considerable impact on the molecular states and their energies and symmetry.

In the following the many-body Hamiltonian given by the sum of the contributions in Eqs. (15) and (17) is diagonalized directly in the Fock space of many-body states. Since the Hamiltonian commutes with the number operator $\hat{N} = \sum_{i\sigma} \hat{n}_{i\sigma}$ and the z projection S_z of the total spin, each of the (N, S_z) subblocks of the Fock space is diagonalized separately. For the neutral $N = 6$ state of the molecule, the dimension of this subblock is 400×400 implying that the Hamiltonian can be diagonalized with standard diagonalization routines. This yields the many-body states

$$|N, i\rangle = \sum_n c_n |\phi_n^N\rangle \qquad (18)$$

and their corresponding energies E_i^N, where $\{|\phi_n^N\rangle\}$ denotes the possible N-electron configurations with spin S_z and c_n are the expansion coefficients. For example, in the singlet ground state of the neutral isolated molecule where the Hamiltonian is given by Eq. (15), the configuration $|\phi_n^{N=6}\rangle = |\uparrow\downarrow\uparrow\downarrow\uparrow\downarrow\rangle$ with the spins aligned oppositely on neighboring sites is the one with the largest weight.

In the following, we will focus on transport through the benzene molecule at positive gate voltages. This corresponds to the situation illustrated in Fig. 3(b), where the affinity level is located in the bias window. Due to the electron-hole symmetry of the PPP Hamiltonian, the transport through the positively charged cation will be identical. The states relevant for the transport at positive gate voltages are illustrated schematically in Fig. 3(a). This includes the ground state of the neutral molecule ($N = 6$) and the degenerate ground state of the singly charged anion ($N = 7$) which is split up by the image charge effect as illustrated in the right plot. The next excited states lie more than 2 eV above these states and will hence not be active under moderate source-drain biases.

B. Addition energy and breaking of degeneracies

The most apparent effect of the interaction with the image charges is a strong renormalization of the molecular charging energies which has been observed both experimentally[6,7] and theoretically.[8,9] This results in a large reduction of the addition

TABLE I. Addition energy (in eV) and splitting Δ (in meV) of the degenerate ground state of the negatively charged anion ($N = 7$) in different situations. The symmetric and antisymmetric configurations correspond to the setups illustrated in Figs. 1(b) and 1(c), respectively. In the rotated setup, the molecule has been rotated by an angle $\theta = \pi/6$ around its sixfold rotational symmetry axis. The reduction of $\sim$3.6 eV for the addition energy in the symmetric and rotated setups is of the same size as the reductions found with *ab initio* GW/DFT calculations for a benzene molecule on a graphite surface (Ref. 35) and in a SET environment (Ref. 36). The smaller reduction observed for the addition energy in the third row is a consequence of the asymmetric setup which reduces image charge effect from the more distant electrode. In the last column the point group symmetry of the Hamiltonian in the absence of an applied bias voltage is given.

	E_{add}	Δ	Symmetry
Isolated	11.38	–	D_{6h}
SET (symmetric)	7.77	72	D_{2h}
SET (asymmetric)	8.01	43	C_{2v}
SET (rotated)	7.73	76	–

energy, given by the difference between the ionization potential (IP) and electron affinity (EA),

$$E_{\text{add}} = \text{IP} - \text{EA} = E_0^{N+1} + E_0^{N-1} - 2E_0^N, \quad (19)$$

compared to its value for the isolated molecule. As shown in the first column of Table I, the addition energy of the benzene molecule is reduced by up to $\sim$3.6 eV in setups similar to those in Fig. 1. This is of the same size as the reductions found with *ab initio* descriptions of the benzene molecule in similar environments.[35,36] Due to the smaller image charge effect from the most distant electrode in the asymmetric setup, the reduction of the addition energy is smaller in this case. Similar reductions of the molecular HOMO-LUMO gaps are expected to occur in single-molecule junctions with a stronger coupling to the leads where coherent transport dominate.[37]

The large renormalization of the molecular energy levels is also manifested in the charge distribution on the molecule where the attractive nature of the oppositely charged image charges polarizes the molecule. The magnitude of this effect can be quantified in terms of the site occupations on the benzene ring which follow from the expectation value $\langle \hat{n}_i \rangle = \langle N | \hat{n}_i | N \rangle$. In the symmetric setup in Fig. 1(b), we find that $\sim$0.3 of the added electron in the anion resides on each of the end atoms closest to the electrodes while only $\sim$0.1 resides on each of the four center atoms. For the exact diagonalization of the Hamiltonian given here, this charge rearrangement corresponds to a change in the weights c_n of the different N-particle configurations in the many-body state compared to the isolated molecule.

In transport measurements, the addition energy can be inferred from the height of the Coulomb diamonds in the charge stability diagram.[38] However, even when taking into account the image charge effect, the addition energy of the benzene molecule is large compared to experimentally accessible source-drain voltages, and hence the observation of full Coulomb diamonds for such a small molecule seems unlikely. We will therefore focus on the *I-V* characteristics

at lower biases, where the image charge effect leaves its fingerprint in the form of an additional molecular level that results from a broken symmetry in the molecule.

The PPP Hamiltonian for the isolated benzene molecule in Eq. (15) belongs to the D_{6h} point group. The symmetry and degeneracies of the different charge states of the PPP Hamiltonian for benzene have been considered in detail in Ref. 11 The symmetry of the ground states for the neutral molecule and the anion is A_{1g} and E_{2u}, respectively, with the latter having a twofold orbital degeneracy on top of its spin degeneracy. The states are illustrated schematically in Fig. 3(a).

When taking into account the image charge effect, the symmetry of the full junction Hamiltonian given by Eqs. (15) and (17) is reduced with respect to that of the isolated molecule. In this case, the symmetry of the junction Hamiltonian reflects the symmetry of the combined molecule plus junction setup. The point groups of the Hamiltonian for the different setups are listed in the last column of Table I. For example, in the symmetric setup in Fig. 1(b), the symmetry is reduced to the D_{2h} point group. As a consequence, the orbital degeneracy of the anion E_{2u} ground state is lifted resulting in a splitting Δ between the symmetry-broken states. The situation is illustrated schematically in the right part of Fig. 3(a) (the labeling of the states is explained in the next section). The splitting of the degenerate anion state is listed in the second column of Table I for the different setups. In all cases, the splitting is of considerable size (40−80 meV). In the regime $k_B T > \Gamma$ considered here, the splitting thus exceeds the level broadening Γ even at room temperature in the Coulomb blockaded junctions. With the distance to the image plane of the electrodes in the symmetric setup increased to $\sim$4 Å, the splitting remains on the order of 10 meV. Hence, irrespective of the exact alignment between the molecule and the electrodes, the splitting is large enough for the split states to appear as individual resonances in the charge stability diagram at sufficiently low temperatures.

In the junction considered here, the electrodes and the gate dielectric affect the molecular symmetry differently. Since the molecule is lying flat on the gate dielectric, it does not break the symmetry of molecule. The image charge effect from the electrodes is therefore most important for the observed lifting of the degeneracies. On the other hand, both the gate dielectric and the electrodes contribute equally to the reduction of the addition energy.[9]

C. Selection rules

The charge transport through the molecule is to a high degree determined by the transition matrix elements in Eq. (11). For molecules with symmetries, group theoretical arguments can be used to derive selection rules for the transition matrix elements between the involved states. The selection rules for the isolated benzene molecule have been considered in detail in Ref. 11. Due to the lower symmetry of the full junction Hamiltonian considered here, the following analysis differs slightly.

For the symmetric setup in Fig. 1(b) the Hamiltonian belongs to the D_{2h} point group. The elements of the point

group and the Hamiltonian therefore posses a common set of eigenstates. Here, the symmetry of interest is the symmetry operation σ_v which is a reflection about the plane through the two carbon atoms closest to the electrodes and perpendicular to the molecular plane. The eigenstates can therefore be classified by the eigenvalues ± 1 corresponding to symmetric and antisymmetric states with respect to reflections in the mirror plane σ_v. The ground state $|0\rangle$ of the neutral molecule is symmetric; i.e., $\sigma_v |0\rangle = |0\rangle$. For the split ground state of the anion, the lower and higher lying states are symmetric and antisymmetric, respectively. We therefore label them as in Fig. 3 where $|s\rangle$ denotes the symmetric and $|a\rangle$ the antisymmetric excited state of the anion.

We now consider coupling in the para configuration where the leads couple to the two atoms facing the electrodes in Fig. 1(b). Since the coupling atoms lie in the mirror plane σ_v, the transition matrix element between the symmetric $N = 6$ ground state and the antisymmetric $N = 7$ state can be shown to fulfill the following equality,

$$\langle N+1,a|c_{\alpha\sigma}^\dagger|N,0\rangle = -\langle N+1,a|c_{\alpha\sigma}^\dagger|N,0\rangle, \qquad (20)$$

implying that the matrix element vanishes.[11] Transitions to the antisymmetric state are therefore forbidden which results in a so-called dark state that cannot be observed in transport measurements. For transitions between the two symmetric states no such restriction exists. In other words, this is a statement that the operator $c_{\alpha\sigma}^\dagger$ preserves the symmetry of the state when coupling in the para configuration. In the meta configuration, where one of the couplings is shifted to the neighboring site, the creation operator for the shifted coupling site no longer preserves the mirror symmetry of the states. Hence, the matrix element will be nonzero for both the symmetric and antisymmetric state of the anion.

Since the mirror symmetry σ_v is an element of the C_{2v} point group, the selection rules derived above also apply in the asymmetric setup in Fig. 1(c). One way to break the mirror symmetry is to rotate the benzene molecule around its sixfold rotational symmetry axis as sketched in Fig. 1(d). This breaks all the symmetries in the molecule and destroys the selection rules for the transition matrix elements. Figure 4 shows the absolute value of the transition matrix elements as a function of the rotation angle θ with respect to the symmetric setup in Fig. 1(b). The matrix elements for coupling to both the para (red lines) and meta (green lines) sites are shown. As evident from Fig. 1, the para coupling sites become the meta site and vice versa under a rotation of $\theta = \pi/3$. For $\theta = \pi/6$ the two coupling sites are equivalent. This is reflected in the mirror symmetry between the red and green lines in Fig. 4 which meet at $\theta = \pi/6$.

As discussed above, the para matrix element vanishes for the antisymmetric state at $\theta = 0$. The other transition matrix elements all have finite values in the nonrotated setup. For $\theta \neq 0$ the mirror symmetry of the junction is broken and the selection rules derived from Eq. (20) no longer apply. As a result, the transition matrix element for the antisymmetric state with coupling at the para site acquires a finite value. Under these circumstances, transport via the otherwise dark state becomes possible. As will be discussed in further detail below, the small magnitude of the associated transition matrix element
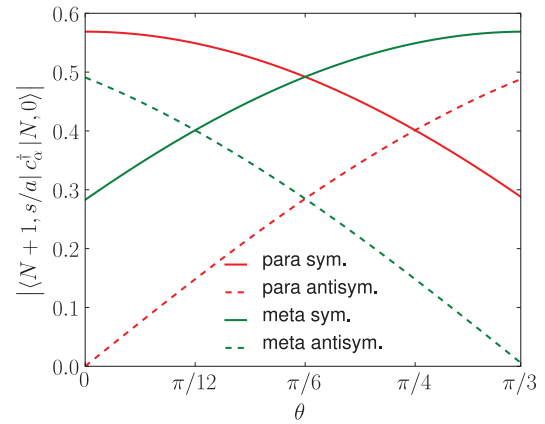

FIG. 4. (Color online) Transition matrix elements $|\langle N+1,s/a|c_{\alpha\sigma}^\dagger|N,0\rangle|$ between the ground state $|0\rangle$ of the neutral molecule ($N = 6$) and the symmetric/antisymmetric state $|s\rangle/|a\rangle$ of the anion ($N = 7$) vs angle of rotation of the benzene molecule. The rotation angle is with respect to the symmetric setup in Fig. 1(b). The red and green lines refer to coupling at the para and meta sites denoted by red and green dots in Fig. 1, respectively.

for the antisymmetric state in Fig. 4 is likely to cause NDR. The occurrence of NDR from a low-lying symmetry-split state may therefore serve as a fingerprint of a broken symmetry in the molecule.

D. Current and NDR

At relatively low biases, only the low-lying states illustrated in Fig. 3(a) will be active in the charge transport through the molecule. More specifically, only the ground state of the neutral molecule and the split degenerate ground state of the singly charged molecule need to be considered. Given that the temperature is low enough and $k_B T > \Gamma$, the large splittings Δ of the anion states in Table I bring the junction outside the quasidegenerate regime $\Gamma \sim \Delta$ where coherence between the degenerate states is important.[11,13] Hence, the out-of-equilibrium occupations of the molecular many-body states and the current can be obtained with the conventional rate-equation approach described in Sec. II C.

With only three states—two of which are the symmetry-split doublets of the singly charged molecule—participating in the transport the stationary rate equations take the simple form

$$\begin{pmatrix} -(\Gamma_{s0}+\Gamma_{a0}) & \Gamma_{0s} & \Gamma_{0a} \\ \Gamma_{s0} & -\Gamma_{0s} & 0 \\ \Gamma_{a0} & 0 & -\Gamma_{0a} \end{pmatrix} \begin{pmatrix} P_0 \\ P_s \\ P_a \end{pmatrix} = 0, \qquad (21)$$

where the 0, s, and a subscripts denote the ground state of the neutral molecule and the symmetric ground state and first excited antisymmetric state of the charged molecule, respectively. The rates $\Gamma_{ij} = \Gamma_{ij}^L + \Gamma_{ij}^R$ have contributions from tunneling to both the left and right leads. For the states of the charged molecule $P_{s/a}$ denotes the occupations of the individual spin up and down states of the doublet which are equal, i.e., $P_{i\uparrow} = P_{i\downarrow} = P_i$. Together with the normalization

condition $P_0 + 2P_s + 2P_a = 1$ the rate equations have the solution

$$P_0 = \frac{\Gamma_{0s}\Gamma_{0a}}{\widetilde{\Gamma}^2} \; ; \; P_s = \frac{\Gamma_{s0}\Gamma_{0a}}{\widetilde{\Gamma}^2} \; ; \; P_a = \frac{\Gamma_{a0}\Gamma_{0s}}{\widetilde{\Gamma}^2}, \quad (22)$$

where $\widetilde{\Gamma}^2 = \Gamma_{0s}\Gamma_{0a} + 2(\Gamma_{a0}\Gamma_{0s} + \Gamma_{s0}\Gamma_{0a})$. The current through the molecule, here evaluated at the left lead, is then given by

$$\begin{aligned} I &= -2e\big[P_0\big(\Gamma_{s0}^L + \Gamma_{a0}^L\big) - P_s\Gamma_{0s}^L - P_a\Gamma_{0a}^L\big] \\ &= 2e\frac{\Gamma_{s0}^R\Gamma_{0a}\Gamma_{0s}^L + \Gamma_{a0}^R\Gamma_{0s}\Gamma_{0a}^L - \Gamma_{0s}^R\Gamma_{0a}\Gamma_{s0}^L - \Gamma_{0a}^R\Gamma_{0s}\Gamma_{a0}^L}{\widetilde{\Gamma}^2}, \end{aligned}$$
$$(23)$$

where the factor of 2 comes from the spin degeneracy of the anionic doublet states.

In the following we wish to establish a general condition for γ factors in Eq. (11) under which NDR occurs for the three-state system of the symmetry-broken benzene molecule. Similar considerations have been given in Ref. 39 for a spinless three-state system. We here generalize this condition to take into account the spin degeneracy of the two anionic states. The result is completely general and can be applied to similar three-state systems which generally occur in single-molecule junctions when an excited state of a charged molecule becomes accessible.[40]

In the case of NDR, the current decreases at the voltage where the excited state enters the bias window. The situation is illustrated schematically in Fig. 3(c). Here, I_s is the current when only the level for the symmetric state of the anion is located in the bias window. For larger values of the bias voltage where the antisymmetric state becomes accessible, the current either increases or decreases to the value I_{sa}. In this case, the current is given by the expression in Eq. (23). In the former case, the Fermi factor in Eq. (10) is zero for the antisymmetric state and the expression for the current simplifies to

$$\begin{aligned} I &= -2e\big[P_0\Gamma_{s0}^L - P_s\Gamma_{0s}^L\big] \\ &= 2e\frac{\Gamma_{s0}^R\Gamma_{0s}^L - \Gamma_{0s}^R\Gamma_{s0}^L}{\Gamma_{0s} + 2\Gamma_{s0}}. \end{aligned} \quad (24)$$

The NDR, illustrated by the (red) dashed line in Fig. 3(c), occurs when $|I_s| > |I_{sa}|$. At the horizontal plateaus in between the jumps in the current, the distance $|E_{s/a} - \mu_\alpha|$ between the molecular levels and the chemical potentials of the leads is assumed to be larger than the thermal energy k_BT. The Fermi factors f_α and $1 - f_\alpha$ in Eqs. (10) and (12) for the rates can therefore be set to either unity or zero. Together with the current expressions in Eqs. (23) and (24), the inequality for the currents above leads to the following conditions for the γ factors:

$$\begin{aligned} \frac{1}{\gamma_{0a}^L} &> \frac{1}{2\gamma_{s0}^R} + \frac{1}{\gamma_{0s}^L} \quad (\mu_L < \mu_R), \\ \frac{1}{\gamma_{0a}^R} &> \frac{1}{2\gamma_{s0}^L} + \frac{1}{\gamma_{0s}^R} \quad (\mu_L > \mu_R), \end{aligned} \quad (25)$$

which must be fulfilled in order to have NDR at positive or negative bias voltage, respectively. These inequalities can be fulfilled when the excited antisymmetric state of the anion is

a so-called blocking state which has a small exit rate; i.e., γ_{0a}^α must be small for the drain electrode compared to at least one of the γ factors for the symmetric state. The existence of such a small exit rate results in a slowing down of the charge transfer dynamics when the corresponding state enters the bias window and is therefore often accompanied by NDR. In Fig. 3(a) the corresponding transition is marked by the (red) dashed arrow. It should be noted that the inequalities above only require the exit rate for the excited state to be small and put no constraint on the in rate.

A situation with a small exit rate can be realized in either of the following two ways (or both). In the case of strongly asymmetric tunnel couplings, e.g., $t_L \ll t_R$, the exit rate becomes small when the coupling to the drain electrode is the weaker. However, given that the transition matrix elements for the states in Eq. (11) are the same, this situation results in a small exit rate for both the symmetric and antisymmetric state and is therefore not sufficient for the occurrence of NDR. A difference in the transition matrix elements between the states in Eq. (11) on top of the asymmetry in the tunnel couplings is therefore required to fulfill the inequalities in Eq. (25). On the other hand, for symmetric tunnel couplings, i.e., $t_L = t_R$, NDR is also possible. Here, the inequalities Eq. (25) may be satisfied by the transition matrix elements alone when the matrix element for the excited state is small. A recent theoretical study has demonstrated that this property can be designed into conjugated molecules by functionalizing them with different types of chemical groups.[40] This results in asymmetric molecular orbitals for the excited states and consequently a small transition matrix element at one end of the molecule that produces NDR. As discussed in the previous section, the small transition matrix element is here provided by the destroyed selection rules in the low-symmetry setup in Fig. 1(d), where the molecule is placed in a rotated configuration.

IV. I-V CHARACTERISTICS AND STABILITY DIAGRAMS

In the following section the I-V characteristics of the different setups is considered. In all cases the temperature of the leads is set to $k_BT = 5$ meV and the equilibrium Fermi level of the leads is positioned in the middle of the molecular gap. Furthermore, since only transport via the negatively charged anion of the molecule is considered, the discussion is restricted to positive gate voltages. It should be emphasized that the many-body states, their energy, and the transition matrix elements in Eq. (11) are calculated for each value of the applied voltages. The I-V characteristics reported in the following therefore include possible shifts of the molecular levels with the applied bias voltage. In particular, different capacitive couplings to the source and drain electrodes arising from the asymmetric setup will result in I-V characteristics that are asymmetric in the bias voltage.

A. Symmetric setup with coupling in the para configuration

Figure 5 summarizes the I-V characteristics of the symmetric setup in Fig. 1(b). Due to the selection rules, the antisymmetric state is not active in the transport for the nonrotated case when coupled in the para configuration.
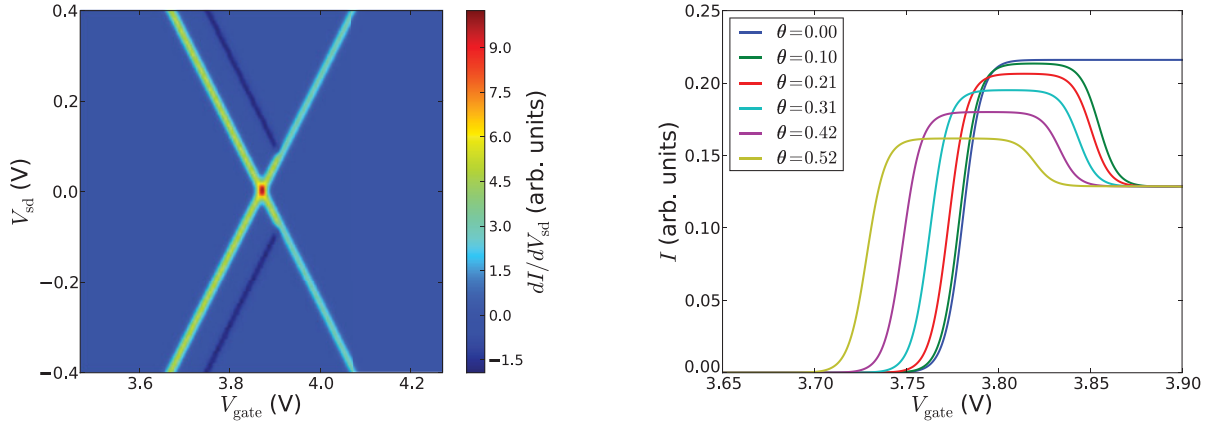
FIG. 5. (Color online) *I-V* characteristic for the symmetric setup and coupling in the para configuration. Left: Stability diagram for $\theta = \pi/12 \sim 0.26$, $k_B T = 5$ meV, and $t_L = t_R$. Right: Absolute value of the current vs gate voltage at $V_{sd} = 0.2$ V for different values of θ. As evident from the blue $\theta = 0$ curve, the selection rules for the transition matrix elements in Eq. (11) completely expel the antisymmetric anionic state from participating in the transport and no NDR is observed. The varying position of the current onset and the current dip is caused by a weak θ dependence of the molecular energy levels.

However, when the molecule is rotated the matrix element for the antisymmetric state acquires a finite value (see Fig. 4) allowing the antisymmetric state to be populated when it enters the bias window. The left plot in Fig. 5 shows the stability diagram for a rotation angle $\theta = \pi/12$ of the benzene molecule and symmetric tunnel couplings $t_L = t_R$. At this value for θ, the ratio between the transition matrix elements for the symmetric and antisymmetric states with coupling to the para site is $|\langle s|c_{\alpha\sigma}^\dagger|0\rangle / \langle a|c_{\alpha\sigma}^\dagger|0\rangle| \sim 3.7$. Reverting to the condition for the occurrence of NDR in Eq. (25), this value for the ratio between the transition matrix elements is found to fulfill the inequalities in the case of symmetric tunnel couplings. Consequently, an NDR feature appears in the stability diagram at the voltages where the antisymmetric state becomes accessible. The right plot in Fig. 5 shows the absolute value of the current as a function of the gate voltage at $V_{sd} = 0.2$ V for different values of the rotation angle of the benzene molecule. Due to the symmetry forbidden population of the antisymmetric state

at $\theta = 0$, this state remains unpopulated at the gate voltage where it enters the bias window. Therefore, the corresponding curve in the right plot of Fig. 5 does not show any change in the current at the corresponding gate voltage. For increasing rotation angles, both the NDR effect and the current level prior to the onset of the NDR is seen to decrease. This trend is a direct consequence of the variation of the transition matrix elements shown in Fig. 4 when the molecule is rotated with respect to the electrodes. Likewise, the shift of the onset for the current and NDR originates from small changes in the level positions when the molecule is rotated.

The linear character of the Coulomb diamond boundaries reveals that the bias voltage does not have any apparent effect on the molecular states and their energies. Only at much higher voltages may this become important. For longer molecules, however, where the voltage drop over the molecule becomes significant, a larger impact on the molecular states is possible.[9] These considerations also indicate that the symmetry-breaking
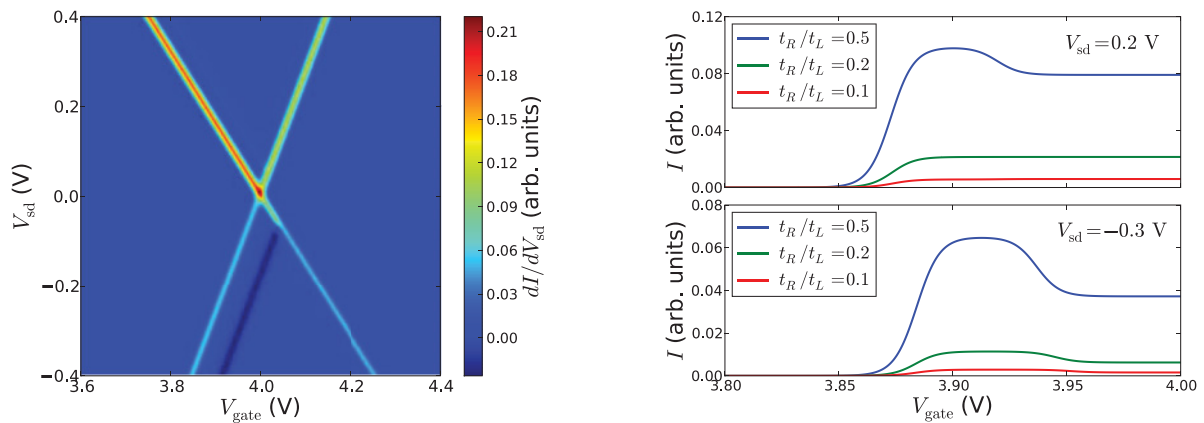

FIG. 6. (Color online) *I-V* characteristics for the asymmetric setup where the distance to the right electrode is twice the distance to the left electrode and with coupling in the para configuration. Left: Stability diagram for $\theta = \pi/12 \sim 0.26$, $k_B T = 5$ meV, and $t_L = 10 t_R$. Right: Absolute value of the current vs gate voltage for different values of the tunnel coupling ratio t_R/t_L at positive and negative bias voltage.
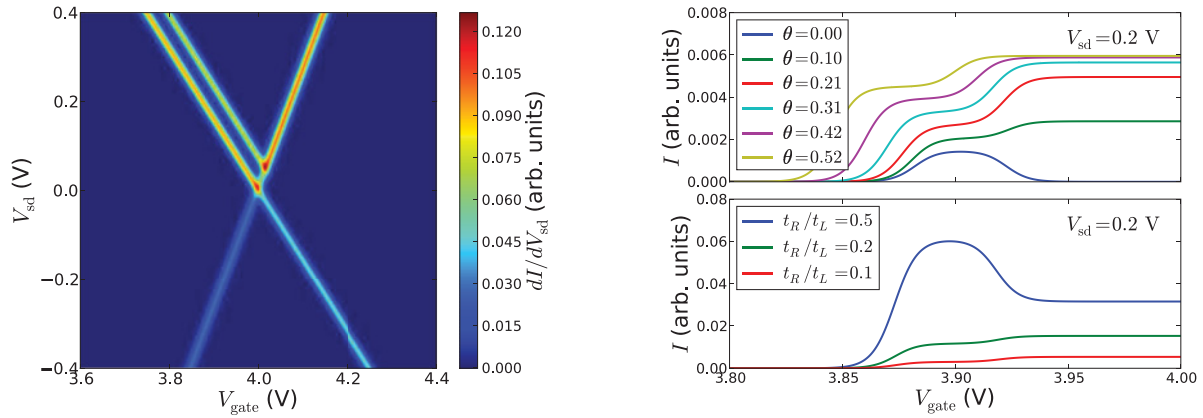
FIG. 7. (Color online) *I-V* characteristics for the asymmetric setup with coupling in the meta configuration. Left: Stability diagram for the same set of parameters as in Fig. 6. Right: Absolute value of the current vs gate voltage for different values of the rotation angle θ at $t_L = 10t_R$ (upper) and the tunnel coupling ratio t_R/t_L at $\theta = \pi/12$ (lower). Note the collapse of the current for $\theta = 0$ in the upper plot.

effect of the bias voltage is here negligible compared to that of the image charge effect.

B. Asymmetric setup with coupling in both para and meta configuration

Next, we focus on the asymmetric setups illustrated in Fig. 1(c). Due to the larger distance to the right electrode it becomes relevant to address the effect of an asymmetry in the tunnel couplings, i.e., $t_L > t_R$, and coupling to the meta site at the right electrode. Since the values of the transition matrix elements in Fig. 4 are left relatively unaffected by the asymmetry of the setup, changes in the *I-V* characteristics as compared to the symmetric setup considered in the previous section can be attributed to the introduced tunnel coupling asymmetry and the change in the coupling site.

1. Coupling in para configuration

Figure 6 summarizes the *I-V* characteristics for the asymmetric setup with coupling in the para configuration. Here, the left plot shows the stability diagram for $\theta = \pi/12$ and $t_R/t_L = 0.1$. Due to the asymmetry of the setup, the different capacitive couplings to the left and right electrodes give rise to different slopes of the diamond edges in the stability diagram.

A clear change in the stability diagram compared to the one for the symmetric setup in Fig. 5 is the disappearance of the NDR feature for positive bias voltages. This behavior follows from the asymmetry in the tunnel couplings. For positive bias voltages the electrons exit the molecule to the left electrode. Depending on the ratio between the transition matrix elements, the asymmetry in the tunnel couplings may result in a large exit rate; i.e., $\gamma_L > \gamma_R$. From the NDR conditions in Eq. (25), one sees that this can remove the NDR. Indeed, for $t_R/t_L = 0.1$ and the previous stated ratio of the transition matrix elements, this is the case. For these parameter values, the difference in the transition matrix elements for the symmetric and antisymmetric states that produced NDR in the case of symmetric couplings is outweighed by the large asymmetry in the tunnel couplings. Hence, the NDR feature is absent at positive bias voltages. On the other hand, for negative

bias voltage where the NDR feature still appears, the exit rate for the antisymmetric state to the right electrode remains small and the lower inequality in Eq. (25) is fulfilled.

Since the tunnel couplings depend exponentially on the distance to the electrodes, other values for their ratio should also be considered. The right plot in Fig. 6 shows current as a function of gate voltage for different values of the ratio t_R/t_L at positive ($V_{sd} = +0.2$ V) and negative ($V_{sd} = -0.3$ V) bias voltage. As expected, the current level and the dip in the current occurring at the position of the NDR feature in the stability diagram are highly dependent on the tunnel couplings. At positive bias, the current dip appears only for the smallest asymmetry $t_R/t_L = 0.5$ in the couplings. From the ratio between the transition matrix elements for the symmetric and antisymmetric state given in the previous section, the value of the ratio t_R/t_L at which no dip in the current is observed can be deduced from Eq. (25). For positive bias, the upper inequality in Eq. (25) becomes an equality at $t_R/t_L \sim 0.2$. At this value for the coupling ratio, the difference in the transition matrix elements has been compensated for by the asymmetry in the tunnel couplings and no change in the current occurs when the antisymmetric state enters the bias window. For smaller values of the coupling ratio, i.e., larger asymmetry in the tunnel couplings, the current increases slightly. Again, at negative bias voltage, the tunnel coupling to the right drain electrode is the smaller and the current dip persists for all the shown values of the coupling ratio.

2. Coupling in meta configuration

Changing the coupling site at the right electrode to the meta site changes things drastically. Figure 7 summarizes the *I-V* characteristics for this case. Again, the left plot shows the stability diagram for the same parameter values as used in Fig. 6. As shown in Fig. 4, the transition matrix elements for coupling to the meta site are equal at $\theta = \pi/12$ for the symmetric and antisymmetric state. This has the immediate consequence that $\gamma_{0a}^R = \gamma_{0s}^R$, implying that the lower inequality in Eq. (25) giving the condition for NDR at negative bias can never be fulfilled. This is reflected in the stability diagram

where no NDR from the antisymmetric state is observed at negative bias. As opposed to the situation with coupling in the para configuration, the resonance from the antisymmetric state now appears at positive bias and gives rise to an increase in the current instead of NDR.

The upper right plot in Fig. 7 shows how the current in the vicinity of this resonance varies with the rotation angle θ. For $\theta = 0$ a complete collapse of the current is observed when the antisymmetric state becomes accessible. From the selection rules discussed in Sec. III C and Fig. 4, we recall that the transition matrix element for coupling to the para site vanishes, while the matrix element for coupling to the meta site is finite. At positive bias this allows the antisymmetric state to become populated from the right electrode. However, since the exit process from the para site at the left electrode is forbidden by symmetry, the molecule remains trapped in the antisymmetric state and the current is blocked. A similar collapse of the current in a benzene SET has been reported in Ref. 20, where the blocking state was populated via radiative relaxation from a higher lying excited state. For $\theta \neq 0$ the current collapse as well as the NDR disappears, and an increase in the current as the one in the stability diagram appears instead.

As in the previous section, the disappearance of the NDR feature in the stability diagram is caused by the large asymmetry in the tunnel couplings. The ratio of the couplings at which the current dip vanishes can be inferred from the upper inequality in Eq. (25). For $\theta = \pi/12$, we find that the condition for NDR is met for $t_R/t_L > 0.41$. The lower right plot in Fig. 7 shows the current as a function of gate voltage at $V_{\rm sd} = +0.2$ for different values of the tunnel couplings. As expected, only the upper blue curve with $t_R/t_L = 0.5$ shows NDR.

V. SUMMARY AND CONCLUSIONS

Using a theoretical framework developed for semiconductor nanostructures, we have studied the impact of the image charge effect on the molecular states and the transport in a benzene single-electron transistor operating in the Coulomb blockade regime. As demonstrated, the image charge effect renormalizes the charging energies and lifts the degeneracy of the twofold orbitally degenerate ground state of the singly charged anion of the benzene molecule. With the resulting splitting of the degenerate states exceeding both the thermal energy $k_{\rm B}T$ and the level broadening Γ from the tunnel coupling to the leads, this has important consequences for the low-bias *I-V* characteristics of the benzene SET. In particular, the selection rules between the transport active many-body states of the molecule are destroyed, which gives rise to the appearance of a blocking state that leads to the occurrence of NDR. From the derived NDR conditions for a generic three-state system, the coming and going of the NDR feature at different parameter values has been analyzed. It is demonstrated that the appearance of the NDR feature is very sensitive to asymmetries in the tunnel couplings to the source and drain electrodes, to the bias polarity, and to changes in the coupling from the para site to the meta site. In experimental situations, observations of the described transport characteristics may be an indication of a broken symmetry in the molecule.

Altogether, we have demonstrated that image charge effects play a potentially important role, not only for the position of the molecular levels, but also for the molecular states and their degeneracies. As mentioned in the introduction, experimental studies[7,10] have already speculated that image charge effects affect spin excitations of molecules. With the exchange coupling in effective spin Hamiltonians being determined by hopping integrals and Coulomb matrix elements between the orbitals, a large impact on spin states could be anticipated.

With the present work, we have paved the way for more detailed descriptions of single-molecule SETs taking into account image charge effects. In this respect, the electrostatic Green's function for the generic junction geometry given in Appendix A and the inclusion of the additional image charge terms in the PPP Hamiltonian in Appendix B provide a good starting point for future studies of the image charge effect in single-molecule junctions.

APPENDIX A: ELECTROSTATIC GREEN'S FUNCTION FOR A GENERIC JUNCTION GEOMETRY

In this appendix we give an analytical solution of Poisson's equation for the electrostatic Green's function in the simplified junction geometry shown in Fig. 8. Despite its simple structure, the Green's function of this junction provides a good description of the potential in more realistic junctions as the one illustrated in Fig. 1.

When solving Poisson's equation in Eq. (6), the screening induced polarization charge of dielectric regions is most often accounted for by the spatially dependent dielectric constant $\varepsilon_r(\mathbf{r})$. In the following a different route will be taken by treating the polarization charge as a source term in Poisson's equation. For the homogeneous gate dielectric in Fig. 8, the polarization charge induced by a unit source charge in $\mathbf{r}'$ will be a surface charge σ that resides on the interface between the dielectric and the vacuum region. The Green's function can therefore be obtained from the following Poisson equation:

$$-\epsilon_0 \nabla^2 G(\mathbf{r}, \mathbf{r}') = \delta(\mathbf{r} - \mathbf{r}') + \frac{\sigma(\mathbf{r})}{e} \qquad (A1)$$

with Dirichlet boundary conditions, i.e., $G = 0$, at the surface of the metallic electrodes. The surface charge on the right-hand side is located in the xz plane $\sigma(\mathbf{r}) = \sigma(x,z)\delta(y)$ and can be obtained as the normal component of the polarization $\mathbf{P}$
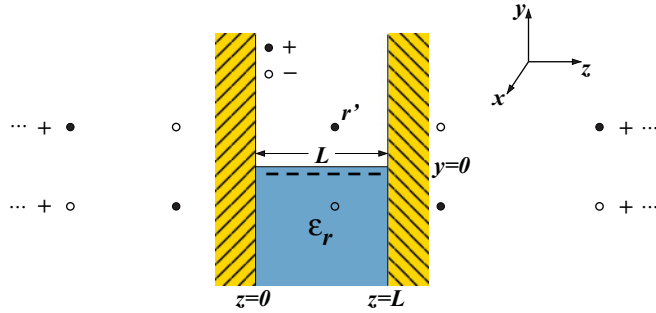
FIG. 8. (Color online) Simple junction geometry for which Poisson's equation can be solved analytically for the electrostatic Green's function. The junction consists of two infinite parallel electrode plates where the lower half space ($y < 0$) between them is filled with an oxide of dielectric constant ε_r. The dots illustrates the image charge solution to Poisson's equation given in Eq. (A5).

at the interface. Using the relations $\mathbf{D} = \epsilon_0 \mathbf{E} + \mathbf{P}$ and $\mathbf{D} = \epsilon_0 \varepsilon_r \mathbf{E}$ between the displacement field $\mathbf{D}$ and the electric field

$\mathbf{E}$ in linear dielectrics, the surface charge can be related to the electric field via

$$\sigma = \mathbf{P} \cdot \hat{\mathbf{n}} = \epsilon_0 (\varepsilon_r - 1) \mathbf{E} \cdot \hat{\mathbf{n}}, \qquad (A2)$$

where the normal component (in this case the y component) is evaluated immediately below the interface, i.e., $y = 0^-$. Expressing the electric field by the gradient of the Green's function, the following relation between the Green's function and the surface charge is obtained:

$$-\hat{\mathbf{n}} \cdot \nabla G(\mathbf{r}, \mathbf{r}') = \frac{1}{\epsilon_0 (\varepsilon_r - 1)} \sigma(\mathbf{r}). \qquad (A3)$$

This relation can be used to eliminate the surface charge in Eq. (A1). The resulting equation for the Green's function is solved by expanding in plane waves and sines as

$$G(\mathbf{r}, \mathbf{r}') = \int \frac{dp}{2\pi} \int \frac{dk}{2\pi} \sum_n \sin \frac{n\pi z}{L} e^{iky} e^{ipx} G(nkp, \mathbf{r}'). \qquad (A4)$$

After much algebra, the following solution for the electrostatic Green's function is found:

$$G(\mathbf{r}, \mathbf{r}') = \frac{1}{4\pi\epsilon_0} \sum_{\sigma=\pm 1} \sum_{\tau=\pm 1} \sigma\tau \left(\frac{\varepsilon_r + \tau}{\varepsilon_r + 1} \right) \left[\frac{1}{\sqrt{(x - x')^2 + (y - \tau y')^2 + (z - \sigma z')^2}} \right.$$
$$\left. + \sum_{n=1}^{\infty} \left(\frac{1}{\sqrt{(x - x')^2 + (y - \tau y')^2 + [2nL - (z - \sigma z')^2]}} + \frac{1}{\sqrt{(x - x')^2 + (y - \tau y')^2 + [2nL + (z - \sigma z')]^2}} \right) \right]$$
$$\equiv \frac{1}{|\mathbf{r} - \mathbf{r}'|} + \widetilde{G}(\mathbf{r}, \mathbf{r}'), \qquad (A5)$$

where $\mathbf{r}, \mathbf{r}'$ belong to the vacuum region of the junction. The solution has the intuitive image charge interpretation illustrated in Fig. 8. The analytic solution in Eq. (A5) allows for a direct identification of the two contributions to the Green's function indicated in the last equality. Here, the direct Coulomb interaction is given by the first term inside the square brackets for $\sigma = \tau = +1$, while the remaining terms give the induced potential $\widetilde{G}$. By comparing to finite element solutions of Poisson's equation (6) in junction geometries as the one illustrated in Fig. 1, we found that the Green's function for the simplified junction considered here to a high degree resembles that of more realistic junctions.

As mentioned in the main text the distances between the atoms of the molecule and the electrostatic boundaries of the junction must be chosen with care. The reason for this is that the positions of the electrostatic boundaries between metallic/dielectric regions and the vacuum region where the molecule resides do not correspond to the actual positions of the atomic surfaces in the junction. Typically, this so-called electrostatic image plane of the atomic surfaces lies ~ 1 Å outside the outermost atomic layer.[28] The distance between the atoms of the molecule and the surface atoms is therefore larger than the chosen distance to the respective image planes.

APPENDIX B: IMAGE CHARGE HAMILTONIAN IN A LOCALIZED BASIS

In this appendix the derivation of the PPP representation in Eq. (17) of the image charge related terms in the junction Hamiltonian in Eq. (3) is outlined.

Within the PPP description, the Hamiltonian is expressed in the basis of the p_z orbitals on the carbon atoms. In this basis the terms related to the image charge effect in Eq. (17) read

$$H_{\text{mol-env}} + H_{\text{env}} = \sum_{ij,\sigma} \widetilde{V}_{ij}^{\text{ion}} c_{i\sigma}^{\dagger} c_{j\sigma} + \frac{1}{2} \sum_{ij,\sigma\sigma'} n_{i\sigma} \widetilde{V}_{ij} n_{j\sigma'}. \qquad (B1)$$

Here, $\widetilde{V}_{ij}^{\text{ion}}$ (> 0) and $\widetilde{V}_{ij}$ (< 0) are the matrix elements of the image charge potential from the ionic cores and the two-electron integrals of the image charge interaction between the electrons. The two types of matrix elements are given by

$$\widetilde{V}_{ij}^{\text{ion}} = \int d\mathbf{r}\, \phi_i^*(\mathbf{r}) \widetilde{V}_{\text{ion}}(\mathbf{r}) \phi_j(\mathbf{r}) \qquad (B2)$$

and

$$\widetilde{V}_{ij} = \int d\mathbf{r} \int d\mathbf{r}' |\phi_i(\mathbf{r})|^2 \widetilde{G}(\mathbf{r},\mathbf{r}')|\phi_j(\mathbf{r}')|^2, \quad \text{(B3)}$$

respectively, where the induced potential from the ions is given by

$$\widetilde{V}_{\mathrm{ion}}(\mathbf{r}) = -\int d\mathbf{r}' \widetilde{G}(\mathbf{r},\mathbf{r}')\rho_{\mathrm{ion}}(\mathbf{r}')$$
$$\approx -\sum_i \widetilde{G}(\mathbf{r},\mathbf{R}_i). \quad \text{(B4)}$$

In the last equality, the charge distribution of the ionic cores have been approximated by δ functions located at the positions $\mathbf{R}_i$ of the carbon atoms in the molecule. Notice that the image potential from the positively charged ions lifts the on-site energy of the electrons. The matrix elements of the image charge interaction between the electrons in Eq. (B3) are negative and therefore correspond to a screening of the direct Coulomb interactions between the electrons.

Here we adopt the level of simplicity of the PPP Hamiltonian and neglect off-diagonal matrix elements of the first term in Eq. (B1) and include only the direct matrix elements of the image charge interaction in the second term. This results in the Hamiltonian in Eq. (17) with the additional terms from the applied voltages treated similarly.

The matrix elements in Eqs. (B2) and (B3) are evaluated by approximating the absolute square of the orbitals by δ functions centered at the atomic sites,

$$\widetilde{V}_i^{\mathrm{ion}} = \int d\mathbf{r}\, |\phi_i(\mathbf{r})|^2 \widetilde{V}_{\mathrm{ion}}(\mathbf{r}) \approx \widetilde{V}_{\mathrm{ion}}(\mathbf{R}_i) \quad \text{(B5)}$$

and

$$\widetilde{V}_{ij} = \int d\mathbf{r} \int d\mathbf{r}'\, |\phi_i(\mathbf{r})|^2 \widetilde{G}(\mathbf{r},\mathbf{r}')|\phi_j(\mathbf{r}')|^2 \approx \widetilde{G}(\mathbf{R}_i,\mathbf{R}_j),$$
$$\text{(B6)}$$

respectively. The matrix elements $\widetilde{V}_{ij}$ obtained for the junction geometry described in the main text are shown in Fig. 2. Also shown are the matrix elements of the direct Coulomb interaction given by the Ohno parametrization in Eq. (16). As the figure shows, the matrix elements of the image charge interaction leads to significant screening of the interactions on the molecule.

* cosby@fys.ku.dk

[1] E. A. Osorio, T. Bjørnholm, J.-M. Lehn, M. Ruben, and H. S. J. van der Zant, J. Phys. Condens. Matter **20**, 374121 (2008).

[2] H. Park, J. Park, A. K. L. Lim, E. H. Anderson, A. P. Alivisatos, and P. L. McEuen, Nature (London) **407**, 57 (2000).

[3] D. R. Ward, G. D. Scott, Z. K. Keane, N. J. Halas, and D. Natelson, J. Phys. Condens. Matter **20**, 374118 (2008).

[4] K. Moth-Poulsen and T. Bjørnholm, Nature Nanotechnol. **4**, 551 (2009).

[5] E. A. Osorio, K. O'Neill, N. Stuhr-Hansen, O. F. Nielsen, T. Bjørnholm, and H. S. J. van der Zant, Adv. Mater. **19**, 281 (2007).

[6] S. Kubatkin, A. Danilov, M. Hjort, J. Cornil, J.-L. Brédas, N. S.-Hansen, P. Hedegård, and T. Bjørnholm, Nature (London) **425**, 698 (2003).

[7] E. A. Osorio, K. O'Neill, M. Wegewijs, N. Stuhr-Hansen, J. Paaske, T. Bjørnholm, and H. S. J. van der Zant, Nano Lett. **7**, 3336 (2007).

[8] P. Hedegård and T. Bjørnholm, Chem. Phys. **319**, 350 (2005).

[9] K. Kaasbjerg and K. Flensberg, Nano Lett. **8**, 3809 (2008).

[10] N. Roch, R. Vincent, F. Elste, W. Harneit, W. Wernsdorfer, C. Timm, and F. Balestro, Phys. Rev. B **83**, 081407(R) (2011).

[11] D. Darau, G. Begemann, A. Donarini, and M. Grifoni, Phys. Rev. B **79**, 235404 (2009).

[12] X. Zhong and J. C. Cao, J. Phys. Condens. Matter **21**, 295602 (2009).

[13] M. G. Schultz, Phys. Rev. B **82**, 155408 (2010).

[14] M. G. Schultz, T. S. Nunner, and F. von Oppen, Phys. Rev. B **77**, 075323 (2008).

[15] T. Frederiksen, K. J. Franke, A. Arnau, G. Schulze, J. I. Pascual, and N. Lorente, Phys. Rev. B **78**, 233401 (2008).

[16] F. Reckermann, M. Leijnse, M. R. Wegewijs, and H. Schoeller, Europhys. Lett. **83**, 58001 (2008).

[17] V. Perebeinos, P. B. Allen, and M. Pederson, Phys. Rev. A **72**, 012501 (2005).

[18] G. Begemann, S. Koller, M. Grifoni, and J. Paaske, Phys. Rev. B **82**, 045316 (2010).

[19] L. D. Hallam, J. Weis, and P. A. Maksym, Phys. Rev. B **53**, 1452 (1996).

[20] M. H. Hettler, W. Wenzel, M. R. Wegewijs, and H. Schoeller, Phys. Rev. Lett. **90**, 076805 (2003).

[21] G. Begemann, D. Darau, A. Donarini, and M. Grifoni, Phys. Rev. B **77**, 201406 (2008).

[22] M. Leijnse and M. R. Wegewijs, Phys. Rev. B **78**, 235424 (2008).

[23] D. J. Griffiths, Introduction to Electrodynamics, 3rd ed. (Prentice Hall, New Jersey, 1999), Chap. 3.

[24] S. S. Datta, D. R. Strachan, and A. T. C. Johnson, Phys. Rev. B **79**, 205404 (2009).

[25] H. Bruus and K. Flensberg, Many-body Quantum Theory in Condensed Matter Physics (Oxford University Press, Oxford, 2004).

[26] E. Bonet, M. M. Deshmukh, and D. C. Ralph, Phys. Rev. B **65**, 045317 (2002).

[27] The bond lengths in the benzene molecule are chosen to be $r_{\mathrm{C-C}} = 1.397$ Å and $r_{\mathrm{C-H}} = 1.1$ Å. As only the p_z orbitals on the carbon atoms are treated explicitly in the diagonalization of the Hamiltonian, the length $r_{\mathrm{C-H}}$ of the bond between C and H only matters for the alignment of the molecule with respect to the electrodes.

[28] S. C. Lam and R. J. Needs, J. Phys. Condens. Matter **5**, 2101 (1993).

[29] R. Pariser and R. G. Parr, J. Chem. Phys. **21**, 466 (1953).

[30] R. Pariser and R. G. Parr, J. Chem. Phys. **21**, 767 (1953).

[31] J. A. Pople, Trans. Faraday Soc. **49**, 1375 (1953).

[32] K. Ohno, Theor. Chim. Acc. **2**, 219 (1964).

[33] R. J. Bursill, C. Castleton, and W. Barford, Chem. Phys. Lett. **294**, 305 (1998).

[34] K. Kaasbjerg and K. S. Thygesen, Phys. Rev. B **81**, 085102 (2010).

[35] J. B. Neaton, M. S. Hybertsen, and S. G. Louie, Phys. Rev. Lett. **97**, 216405 (2006).

[36] K. Stokbro, J. Phys. Chem. C **114**, 20461 (2010).

[37] K. S. Thygesen and A. Rubio, Phys. Rev. Lett. **102**, 046802 (2009).

[38] J. M. Thijssen and H. S. J. van der Zant, Phys. Status Solidi B **245**, 1455 (2008).

[39] B. Muralidharan and S. Datta, Phys. Rev. B **76**, 035432 (2007).

[40] M. Leijnse, W. Sun, M. B. Nielsen, P. Hedegård, and K. Flensberg, J. Chem. Phys. **134**, 104107 (2011).